Norbornene-functionalised chitosan hydrogels and microgels via an unprecedented photo-initiated self-assembly for potential biomedical applications

Sarah Michel[†], Alice Kilner[†], Jean-Charles Eloi[‡], Sarah E. Rogers[§], Wuge H. Briscoe[†], M. Carmen Galan[†]**

[†] School of Chemistry, University of Bristol, Cantock's Close, Bristol BS81TS, UK

[‡] Chemical Imaging Facility, School of Chemistry, University of Bristol, Cantock's Close, Bristol BS81TS, UK

[§] ISIS Neutron and Muon Source, Science and Technology Facilities Council, Rutherford Appleton Laboratory, Didcot, OX11 0QX, UK

KEYWORDS. Polysaccharides, hydrogels, microgels, self-assembly, chitosan

ABSTRACT. Access to biocompatible self-assembled gels and microgels is of great interests for a variety of biological applications from tissue engineering to drug delivery. Here, the facile synthesis of supramolecular hydrogels of norbornene (nb)-functionalised chitosan (CS-nb) via UV-triggered self-assembly in the presence of Irgacure 2959 (IRG) is reported. The *in vitro* stable hydrogels are injectable and showed pH-responsive swelling behaviour, while their structure and mechanical properties could be tuned by tailoring the stereochemistry of the norbornene derivative (e.g. *endo*- or -*exo*). Interestingly, unlike other nb-type hydrogels, the gels possess nanopores

within their structure, which might lead to potential drug delivery applications. A gelation mechanism was proposed based on hydrophobic interactions following the combination of IRG on norbornene, as supported by ^{1}H NMR. This self-assembly mechanism was used to access microgels of size 100-150 nm which could be further functionalised and showed no significant toxicity to human dermofibroblast cells.

I. INTRODUCTION

Supramolecular hydrogels result from self-assembly of physically or reversibly covalently interacting macromolecules or small molecules in solution.[1] These materials have generated tremendous interests in tissue engineering, wound healing and drug delivery applications, due to their intrinsic self-healing properties, their shear-thinning behaviours which are relevant to 3D printing or for *in situ* applications, and their possible responsiveness to a range of stimuli such as pH or temperature.[2-6] Most self-assembled hydrogels exploit hydrophobic interactions between hydrogelators, of which some of the most common examples are aromatically-N-substituted dipeptides (a low molecular weight gelator),[4, 7] amphiphilic polymers,[8] and inclusion complexes.[9] Light is a very attractive stimulus as it provides an additional spatio-temporal control over the self-assembly process,[3] however, examples of light-triggered supramolecular materials are mostly limited to the photo-switchable azobenzene moiety, alone or in cyclodextrin inclusion complexes,[10] and are known to lack stability due to the retro-isomerisation of azobenzene under physiological conditions.[11] Examples of photo-initiated self-assembled polysaccharide hydrogels and materials are rare, with few examples using azobenzene-functionalised hyaluronic acid,[12] cellulose,[13] xylan[14] or dextran.[15]

The development of polysaccharide-based materials has been a very active area of research over the last few years, mainly owing to their low-cost, abundancy, non-toxicity, and natural bioactivity. In addition, the high level of functionality of these biopolymers allows for the incorporation of additional moieties for a specific need.[16, 17] In particular, polysaccharide-based hydrogels and microgels, obtained by either physical or covalent crosslinking of polymer chains in water, have shown promising applications in drug delivery and tissue engineering.[18-21] As opposed to nanoparticles, microgels are soft, deformable and can swell or de-swell in response to the environment while retaining their 3D structure.[22] Their application in the biomedical area takes advantage of their highly swollen core which can be loaded with drugs and biological molecules to protect and slowly release them.[23] More recently, they have also been incorporated into macroscopic hydrogels for enhanced functionality and properties.[24]

Chitosan (CS) is the only cationic natural polysaccharide consisting of β-1,4-D-glucosamine (GlcN) and β-1,4-N-acetyl-D-glucosamine (GlcNAc) units. CS is generally obtained by deacetylation of at least 50 % of GlcNAc residues of chitin.[25] The presence of free amines imparts CS with neuroprotective properties,[26] mucoadhesion, hemostatic action and antibacterial activity, while its similarities with glycosaminoglycans (GAGs) provide a favourable environment for cell adhesion or proliferation.[27-30] In addition, CS can be readily functionalised using its amine group, which has been extensively exploited for application in tissue engineering, wound healing, and drug delivery.[27-29, 31]

Herein we report the facile synthesis of a new class of supramolecular hydrogels and microgels of norbornene (nb)-functionalised chitosan (CS-nb) via UV-triggered self-assembly in the presence of a photoinitiator. The injectable hydrogels exhibit a pH-responsive swelling behavior which is dependent on the stereochemistry of the pendant norbornene and the gels feature

nanopores within their structure, which might lead to potential drug delivery applications. Moreover, we show that the microgels can be further functionalised and showed no significant toxicity to human dermofibroblast cells.

2. EXPERIMENTAL SECTION

Chitosan (CS, low molecular weight 50-190 kDa, deacetylation degree = 76 % calculated by ^{1}H NMR), 5-norbornene-*endo*-2,3-dicarboxylic anhydride (CA-*endo*), 5-norbornene-*exo*-2,3-dicarboxylic anhydride (CA-*exo*) were purchased from Sigma-Aldrich. (3aR,4S,7R,7aS)-hexahydro-4,7-methanoisobenzofuran-1,3-dione (CA-*h*, which corresponds to the hydrogenated form of CA-*endo*) was purchased from Fluorochem. Eosin-5-isothiocyanate was obtained from Insight Biotechnology. Tet-Coum was synthesized as previously reported.[32] Other reagents were purchased from Sigma, Acros, Fluka or Lancaster and used as received. Dialysis against dionised (DI) water (MilliQ; resistivity 18.2 MW cm and total organic content (TOC) < 4 ppb) were performed using a SnakeSkin dialysing tubing with a molecular weight cut-off (MWCO) of 10 kDa (Thermo Scientific). All cell reagents were purchased from ThermoFisher.

^{1}H NMR of CS samples - prepared in D_2O - were recorded with a Varian VNMR S600 Cryo at 40 °C to sharpen the water peak and to allow for more accurate integration of the norbornene peaks. Small molecule ^{1}H NMR were recorded with a JEOL ECZ 400 spectrometer. UV-mediated photoclick reactions were performed with a UV-B lamp (280-320 nm, PL-L 36W/10 2G11, Philips).

2.1 Synthesis of chitosan-functionalised norbornene (CS-nb-*endo*, CS-nb-*exo* and CS-nb-*h*)

CS-nb derivatives were synthesized as previously described.[32] Briefly, CS (1 g, 5.9 mmol) was dissolved in 100 mL of 2% acetic acid (AcOH) in DI water. Once solubilised, the desired carbic

anhydride (CA-*endo*, CA-exo or CA-*h*, 5.9 mmol) was added, and the mixture was stirred at 50 °C for 2 days. The resulting polymer conjugates were dialysed against 5% NaCl for 24 hrs followed by dialysis in DI water for 2 further days, and then lyophilised. The degree of functionalisation (DF in μmol of nb/mg of CS-nb) were calculated by ^{1}H NMR by dissolving 2-to-5 mg of CS-nb in D_2O containing 1 mM of anhydrous DMF used as a standard as reported by Ooi *et al.*[33] A detailed calculation can be found in **Figure S1**.

2.2 Hydrogel synthesis

CS-nb-*endo* and -*exo* was dissolved in 0.1 % IRG in DI water or in 2 % AcOH to a final concentration of 0.5, 1, 2 or 4 w:v%. The mixture was transferred in a sealed glass vial (dimensions: l = 36mm, d_{outer} = 11 mm), vortexed and cured by direct exposure on top of a UV-B lamp (distance lamp – sample ~ 0 mm). The UV time exposure was varied between 20 sec to 1 hr. Hydrogel formation was assessed by the vial-inverted method as described below. At the desired time-scale, the sample curing was stopped, and the sample was inverted. If the material flowed the curing was prolonged for a desired period of time. The sample was finally inverted overnight and was called "gel" if a set material was obtained after 16hrs or "viscous liquid" if not. *Endo*- and *exo*- CS hybrid hydrogels were obtained by the same method mixing CS-nb-*endo* and -*exo* by varying the volume fraction of CS-nb-*endo* ϕ_{endo}. Covalent hydrogels were obtained by mixing CS-nb solutions with thiolated diethylene glycol (HS-DEG-SH) (molar ratio [SH]:[nb] = 1) prior to UV crosslinking.

2.3 Microgel synthesis

Both microgels were synthesized using a previously reported low-energy nano-emulsion template.[32] Briefly, CS-nb-*endo* or -*exo* was dissolved in 0.1 % IRG in 2 % AcOH to a final concentration of 2 w:v%. The resulting solution was added dropwise to a stirred mixture of

cyclohexane containing Span 80 and Tween 80. The nano-emulsion final composition was 10 wt% water phase, 80 wt% oil phase, 4 wt% Span 80 and 6 wt% Tween 80. The mixture was stirred for 30 min on a hot plate and cured with UV-B for 30 min. The microgels were recovered by centrifugation (4000 rpm, 1 hr) and subsequently washed in a VivaSpin®20 concentration centrifugation tube (10 kDa cut-off) with ethanol and water mixes (3x, 1hr 4000 rpm) and water (3x, 1 hr 4000 rpm). The microgels were collected in a glass vial and the concentration was determined by freeze-drying a 50 μL aliquot. The microgel dimensions and ζ potentials were measured using a Malvern Nano Zetasizer zs with a 633 nm laser. Autocorrelation functions were measured at a scattering angle of 173° at 25 °C and processed using the Malvern software package.

2.4 Fluorescent labelling of CS-nb microgels

The desired microgel (4 mg/mL, 1 mL) was reacted with Eosin thioisocyanate (0.2 mg in 2 μL DMSO, 5 w:w% of microgels) by stirring at 700 rpm at room temperature protected from light for 24 hrs. The microgels were dialysed against 1:1 EtOH:H_2O mixture for 24 hrs, 5% NaCl for 24 hrs,and DI water for 24 hrs in a SpinDialyzer chamber (Harvard Apparatus) sealed with a SnakeSkin 10 kDa cut-off membrane. The microgels were collected in a 1 mL plastic tube and the concentration was determined by freeze-drying a 100 μL aliquot.

2.5 Mechanistic studies – polymer scale

Mechanistic investigations were performed with CS-nb-*exo* as the alkene peaks of nb appeared as a singlet. CS-nb-*exo* (75 mg, 37.5 μmol nb) was dissolved in 2 % AcOH (2 mL) with IRG (7.5 mg, 33 μmol) and the resulting mixture was cured with UV-B for 3.5 hrs. At this concentration no hydrogel was formed, and the reaction mixture gradually turned from a transparent solution to a light-yellow solution, confirming the cleavage of IRG. The resulting solution was dialysed in 5% NaCl for 1.5 days and DI water for 3 days to remove unconjugated IRG and lyophilized. The

polymer structure was studied by ^{1}H NMR. To assess the role of AcOH, the kinetics of degradation of IRG (4 mg, 18 µmol) under UV was monitored by ^{1}H NMR in D_2O or 2% AcOD-*d*$_4$ (550 µL) by exposing the NMR tube to UV for 1, 2 or 10 min.

2.6 Mechanistic studies – model system

In situ ^{1}H NMR was used to study the impact of pH and the reactivity of CA-*endo*/*exo*. Briefly, CA-*endo* or -*exo* (5.2 mg, 31.8 µmol) was combined with IRG (10.7 mg, 48 µmol) in DMSO-*d*$_6$ (550 µL). To study the impact of pH, AcOD-*d*$_4$ (11 µL, final concentration 2%) was added to some solutions as a control. The resulting mixtures were transferred in an NMR tube and exposed to UV-B. At defined time points (0, 1 and 2 hrs) the curing was stopped and ^{1}H NMR of the mixture was performed. The reaction was monitored by comparing the integration of the alkene peaks with the singlet of IRG at 1.38 ppm which shifts to 2.08 ppm upon irradiation. The total integration of these two singlets was maintained to 6 for quantification.

2.7 Swelling ratio

Hydrogel samples were realised by curing 200 µL of precursor solution in a centrifuge plastic tube (2 mL) with UV B for 10 min. The resulting hydrogels were lyophilised and the dried mass, w_d, was recorded. Freeze-dried samples were immersed in the desired solution (DI water, PBS, or DI water with pH adjusted to 3 or 11 with 0.1 M HCl or NaOH). The samples were swelled for 7 days, after which the excess of liquid was wiped with filter paper and the mass of the swollen hydrogel, w_s, was recorded. The swelling ratio *SR* was calculated as:[34, 35]

$$\textit{Swelling ratio: } SR = \frac{w_s}{w_d} \quad (1)$$

2.8 SEM images

Hydrogels samples (200 µL) were lyophilised and sectioned through the whole sample before mounting to an aluminium stub. Microgel samples (0.1 mg/mL) were drop-casted on a mica

substrate and dried overnight. Both samples were coated with silver. Images were recorded on a JEOL JSM-IT300 SEM under high vacuum at 15.0 kV. Pore size measurements were performed with ImageJ on an average of 5 to 10 pores randomly taken from 4 images.

2.9 Small angle neutron scattering (SANS)

SANS was carried out on the Sans2d small-angle diffractometer at the ISIS Pulsed Neutron Source (STFC Rutherford Appleton Laboratory, Didcot, U.K.).[36, 37] A simultaneous Q-range of 0.0015 – 0.49 $Å^{-1}$ was achieved utilizing an incident wavelength range of 1.75 – 12.5 Å and employing an instrument collimation length of 12 m, with the 1 m^2 detector offset vertically 75 mm and sideways 100 mm. Hydrogels were prepared in water tight sample cell with its design based on the sample cells available on the D22 beamline at the ILL facility (Grenoble) by curing a solution of CS-nb (2 w:v%) dissolved in 0.1 % IRG/1% AcOD-d_4 in D_2O. The beam diameter was 8 mm. Each raw scattering data set was corrected for the detector efficiencies, sample transmission and background scattering and converted to scattering cross-section data ($\partial\Sigma/\partial\Omega$ vs. Q) using the instrument-specific software.[38] These data were placed on an absolute scale (cm^{-1}) using the scattering from a standard sample (a solid blend of hydrogenous and perdeuterated polystyrene) in accordance with established procedures.[39] Samples were measured at 25°C. Data were background corrected with the scattering of an empty cell. The processing was performed with SasView 4.1.2 software.

2.10 Rheology

Rheological measurements on the obtained hydrogels were performed with a Kinexus rheometer using a parallel plate geometry P20 (d = 20 mm) and a Peltier system for temperature control. The gel samples were synthesized in a 3D-printed PLA mould (diameter 21.5 mm, height 5.9 mm)

from 800 µL of a pre-mixed solution of CS-nb (1, 2 or 4 w:v%), IRG (0.1 w:v%) and the chosen crosslinkers ([SH]:[nb] molar ratio R_s = 1:4, 1:2, 1:1.3 or 1:1) in 2% AcOH. Curing was performed with a UV-B lamp for 15 min on the Peltier plate. The PLA mould was carefully removed, and the hydrogel sample was loaded at a normal force of 0.1 N (typical gap: 1.7 – 2 mm). Dynamic strain sweeps were performed at 1 Hz by varying the strain γ from 0.1 to 100 % at 25°C. Frequency sweep measurements were performed at a shear strain of 1 % by varying the frequency from 10 to 0.1 Hz. All measurements were performed in triplicates. The crosslinking density ρ_s and the mesh size ξ_a were respectively calculated as:[34]

$$\rho_s = \frac{G'}{RT} \tag{2}$$

$$\xi_a = \sqrt[3]{\frac{6}{\pi \rho_s N_A}} \tag{3}$$

2.11 Microgel functionalisation

Microgel functionalisation was performed using a self-quenching fluorescent tetrazine, Tet-Coum, as previously reported.[32] Briefly, the microgels were resuspended in DI water at a final concentration of 0.1 mg/mL in a quartz cuvette (1 cm path length), to which Tet-Coum was added to a final concentration of 1 µM. The reaction was monitored by fluorescence spectroscopy using a PerkinElmer LS45 fluorimeter with an excitation at 420 nm. The emission spectra were recorded in the wavelength range of 460−600 nm.

2.12 Cytotoxicity assays

Human dermal fibroblasts (HDF) were cultured in Minimal Essential Medium (MEM) supplemented with GlutaMAX™, 10% fetal bovine serum (FBS), and antibiotic-antimycotic (AntiAnti). Confluent cultures were detached from the surface using trypsin (Tryp LE Express) before experiments and plated at 5×10^3 cells/well in 96-well plates. The cells were incubated 24

h after plating with microgels at concentrations varied between 500 and 1 µg/mL (4 replicates per condition, i.e., toxicant concentration and time point, all performed in triplicates) for 1 or 2 days. At the required incubation time, the medium was removed and wells were rinsed twice with phosphate buffer saline (PBS). Metabolic activity and cell viability were measured by feeding the cells with FBS-free medium containing 5% Alamar Blue (AB, metabolic activity) and 3 µM Calcein AM (cell viability) for 1 h. Fluorescence was recorded with a CLARIOstar plate reader (AB excitation 515− 555 nm, emission 510−530 nm; Calcein AM excitation 414−483, emission 510−530 nm). All results were background-corrected with a solution of media containing the two dyes and expressed as a percentage of control consisting of cells not exposed to microgels.

2.13 Microgel cell uptake

HDF were seeded in a 96-well plate as described in 0 for 24 hrs and incubated with 0.1 to 0.01 mg/mL of Eosin Y-labelled CS-nb-*exo* microgel for 24 hrs. Wells were rinsed twice with PBS and incubated with 5 µg/mL of CellMask™ deep red plasma membrane stain for 10 min at 37°C. The staining solution was removed, wells were rinsed twice with PBS and the cells were fixed for 10 min with 4% paraformaldehyde. Wells were rinsed twice and nucleus were stained with 300 nM (0.1 µg/mL) DAPI in PBS. Plates were stored in live cell imaging solution at 4°C and imaged at 37°C by widefield microscopy using a Leica LASX live cell imaging workstation equipped with a Leica DFC365FX monochrome CCD camera (1392x1040 6.45µm pixels, 8 or 12-bit, 21 fps full frame). Excitation filters were chosen as 350/50, 545/26 and 620/60 respectively to visualise DAPI, Eosin Y or CellMask™ deep red stains. Data were collected with Leica LAS-X acquisition software.

3. RESULTS AND DISCUSSION

We have previously reported the synthesis of norbornene (nb) functionalised CS (CS-nb) which readily generated covalent hydrogels in the presence of a thiol crosslinker (thiolated diethylene glycol, HS-DEG-SH) with Irgacure 2959 (IRG) as photoinitiator under UV.[32] The nb moiety was introduced to CS by ring-opening of carbic anhydride (CA), conferring an additional carboxylate group which improves CS water solubility, as well as the nb moiety for spatio-temporal control of rapid hydrogel formation (in seconds) through thiol-ene chemistry. However, since commercial CA results from the Diels-Alder cycloaddition of cyclopentadiene and maleic anhydride, it commonly exists as a mixture of two diastereoisomers, *endo* and *exo*. In our efforts to design biomaterials with improved hydrogel network homogeneity, we aimed to study the effect of derivatising CS with pure either *endo*- or *exo*-CA.

To this end, CS-nb-*endo* and -*exo* were synthesized as the pure isomers starting from either CA-*endo* or -*exo* following the procedure we previously described[32] (**Scheme 1**). The nb-functionalisation was proved by ^{1}H NMR with the incorporation of alkene protons, observed as a broad doublet at 6.2-6.3 ppm (peak width = 65.6 Hz) for CS-nb-*endo* and a broad singlet at 6.5 ppm (peak width = 77.3 Hz) for CS-nb-*exo*, while the covalent interaction was confirmed by diffusion ordered spectroscopy (DOSY) (**Figure S1**-**S4**). The degree of functionalisation, assessed using DMF as an internal standard, was determined to be 0.59 and 0.55 μmol nb/mg CS for CS-

nb-*endo* and -*exo*, respectively.

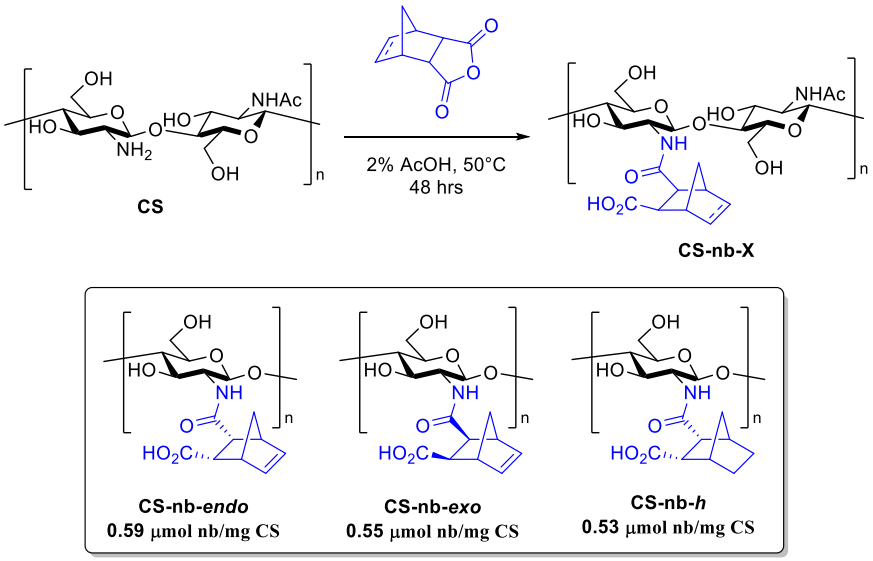

Scheme 1. Synthetic route to CS-nb derivatives and the corresponding chemical structures of CS-nb-*endo*, CS-nb-*exo* and CS-nb-*h*.

Initial attempts to generate hydrogels upon UV exposure with IRG and HS-DEG-SH both in water and under acidic conditions, as previously reported,[32] readily afforded both CS-nb-*endo* and -*exo* hydrogels, respectively. However, unexpectedly, a soft hydrogel was observed for both CS-nb functionalised polymers, when they were cured in acidic conditions with UV and IRG, but in the absence of a thiol crosslinker (**Table S1**). The resulting materials could be shaped in a mould and extruded through a needle to give cylindrical structures, which suggests potential applications in 3D printing or where injectability is required. In contrast, when CS-nb-*endo* was covalently crosslinked with HS-DEG-SH, the gel broke into pieces under shear and could not be extruded through a needle. To the best of our knowledge, such hydrogels obtained from nb-polymers in the absence of a ruthenium catalysts or a thiol crosslinker have never been reported before.

Further investigations showed that hydrogel formation was dependent on the concentration of both CS-nb isomers and IRG, with a minimum polymer concentration of 2 w:v% and a critical IRG concentration of 1 mg/mL for CS-nb-*endo*; CS-nb-*exo* gelation on the other hand was not impacted by IRG concentration. Interestingly, mixtures of CS-nb-*endo* and -*exo* also resulted in hydrogel formation when IRG concentration was maintained to 1 mg/mL (**Figure 1**).

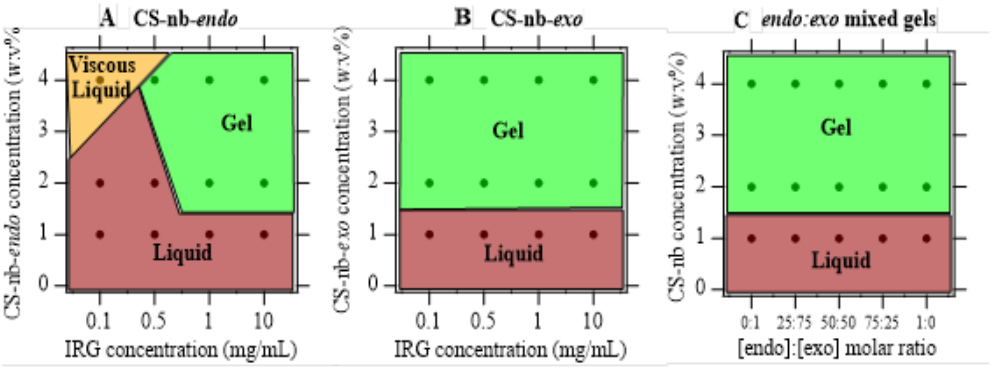

Figure 1. Gel phase diagram of CS-nb-*endo* (**A**), -*exo* (**B**) and of their mixtures (**C**).

To better understand the gelation mechanism, *in situ* ^{1}H NMR experiments were used to demonstrate the covalent bonding of IRG to CS-nb-*exo*. ^{1}H NMR confirmed a decrease of the relative intensity of the alkene peaks (6.5 ppm) of the nb moiety compared to the IRG methyl signals, which shifted from 1.38 to 2.08 ppm after photodegradation. After extensive dialysis of the hydrogels, a broad doublet was found at around 7 ppm, which can be assigned to the covalently attached IRG aromatic moiety confirming the incorporation of IRG to the polymer (**Figure S5**). Furthermore, DOSY indicated the presence of a single species in solution (**Figure S6**). Gelation was thus attributed to the recombination of IRG radicals, following UV irradiation, with the norbornene alkene moiety, leading to the formation of new hydrophobic segments which self-assembled to minimise water exposure, thus acting as crosslinking points between polymer chains

(**Figure 1AB**). IRG contains an aromatic core which may provide additional π-stacking to contribute to crosslinking in gelation. This event is less likely to occur in the presence of thiols due to the very high reactivity of thiol radicals compared to alkene radicals. The formation of nb radicals is known to either occur at the alkene bond or at the bridged position.[40] To assess the reactivity centre CS-nb-*h,* a hydrogenated form of CS-nb, (**Scheme 1**) was synthesized and subjected to the gelation conditions as above. No hydrogel was formed under curing conditions (**Table S1**), further demonstrating that the reactivity observed can be attributed to the alkene functionality. AcOH was thus hypothesized to act as a catalyst either in IRG dissociation or in the radical combination step.

To explore the different gelation ability of CS-nb-*endo* and -*exo*, the reactivity of both CA-*endo* and -*exo* towards IRG was evaluated by *in situ* ^{1}H NMR. After 1 h, almost all the IRG methyl signals shifted to 2.08 ppm while the intensity of the alkene signals of CA-*exo* decreased by 80%. On the other hand, CA-*endo* was less reactive, as evidenced by a decrease in the intensity of the alkene signal of 28% after 1 hr and 55% after 2 hrs (**Figure 2** and **Figure S7** and **S8** in ESI for full spectra). This difference in the reactivity is consistent with the greater ability of CS-nb-*exo* to form hydrogel. In the absence of acetic acid (AcOH), CA-*endo* signals had decreased by 53% after 1 h (**Figure S9**). We thus suggest that AcOH allows for the protonation of CS-nb carboxylic acid group, leading to a more hydrophobic network and thus favouring hydrogel formation, which is not allowed if carboxylate ions are present in water.

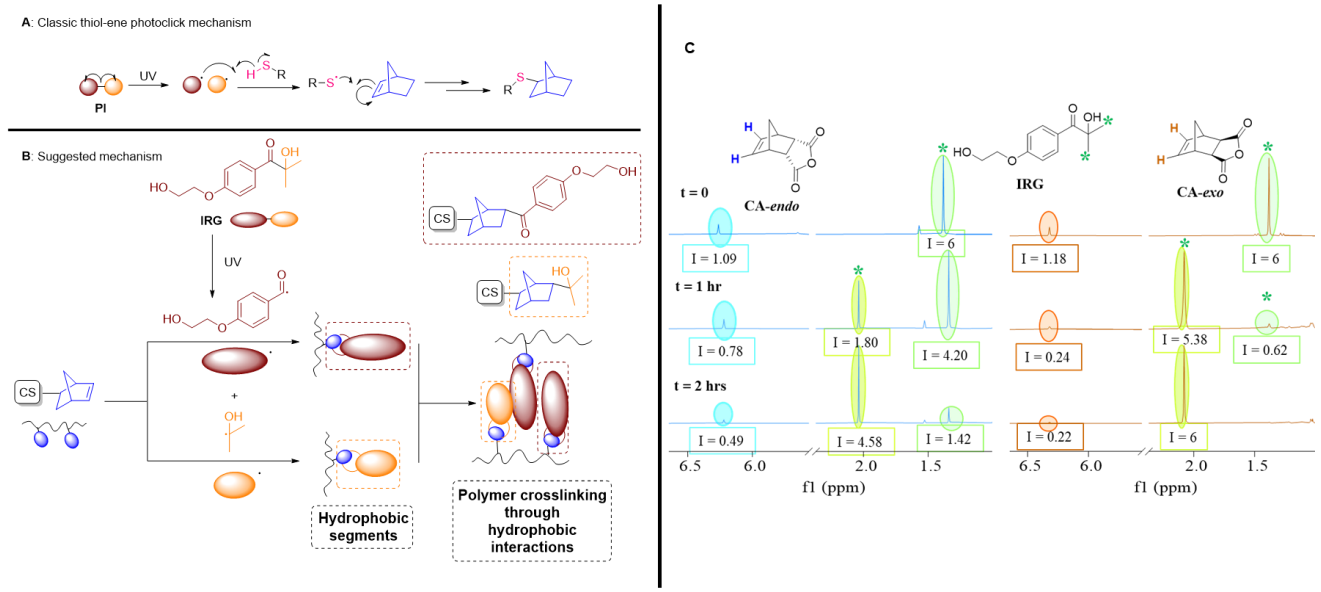

Figure 1. Thiol-ene mechanism (**A**) and proposed reaction mechanism for hydrogel formation (**B**). The photoinitiator IRG is cleaved under UV exposure to give two radicals which react with the nb side-chains of CS, resulting in the incorporation of hydrophobic fragments leading polymer self-assembly driven by hydrophobic interactions and, in turn, to hydrogel formation. ^{1}H NMR studies (**C**) of the reactivity of *endo*- (left, blue) and *exo*-CA (right, brown) with IRG (green) in 2% AcOD-d_4/D_2O.).

The properties of these hydrogels were further investigated for a fixed composition of 2 w:v% CS and 1 mg/mL IRG in 2% AcOH. CS-nb-*endo* hydrogels presented swelling ratios twice as high as the corresponding nb-*exo* derived polymers (**Figure 3**A). This effect was increased under acidic conditions, but decreased drastically in the presence of base or salts, as anticipated for weak polybases.[41] As a comparison, the swelling ratio of a hydrogel obtained from the covalent crosslinking of CS-nb-*endo* with HS-DEG-SH was 2- to 4-times lower even when fully swollen under mild acidic conditions, consistent with enhanced chain mobility in the non-covalent hydrogels.

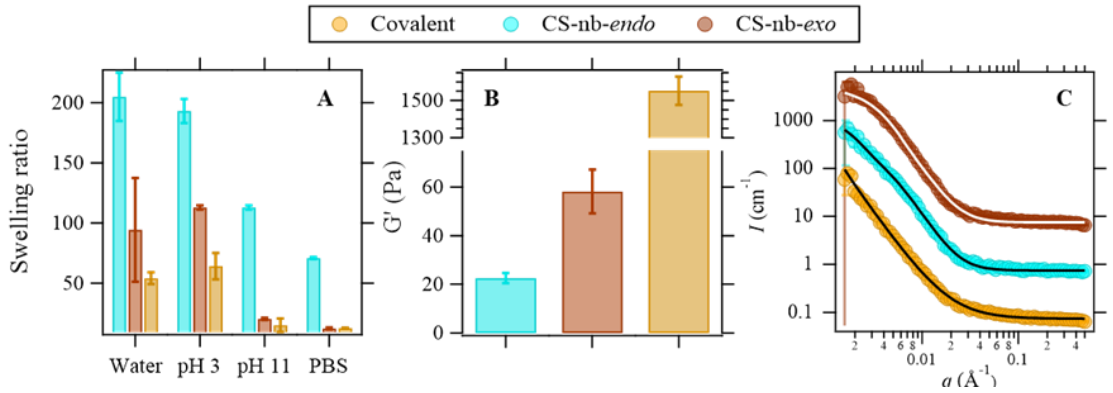

Figure 3. Swelling ratio (A), averaged G' (B), and SANS curves (C) of CS-nb-*endo* and *exo* hydrogels compared to a covalent network, with the fits shown as solid lines. The SANS data has been offset on the y-axis for clarity.

Rheology further confirmed the soft nature of these hydrogels, with G' = 65 and 40 Pa for the *exo* and *endo* materials, respectively, compared to G' ~ 1.1 kPa for the covalent network (**Figure 3B**). By changing CS and IRG concentrations as well as nb stereochemistry, G' could be tuned between ~ 6 to ~ 800 Pa (Figures S10). All -*endo* materials were weaker than the -*exo* derivatives of the same composition. This agrees with the in situ ^{1}H NMR results above that showed the reactivity of IRG and the alkene group was greater with CA-*exo* than CA-*endo*. This could then result in more crosslinking points being formed with the former, thus improving its mechanical properties. Higher IRG concentrations decreased G' of CS-nb-*endo* hydrogels, possibly due to competitive IRG radical degradation or recombination leading to side products, thus reducing the effective formation of crosslink points. Intermediate G' values could be obtained by mixing CS-nb-*endo* and -*exo* before crosslinking (**Figure S11**).

Scanning electron microscopy (SEM) was used to evaluate the hydrogel internal structure (**Figure 4**). All hydrogels presented a porous internal structure, with polydisperse pore sizes of ~ 30 - 150 µm. Interestingly, both CS-nb-*endo* and -*exo* presented internal nanopores with diameters estimated by SEM of respectively ~ 60 and ~ 40 nm. This feature was not observed in the

covalently crosslinked CS-nb-*endo* hydrogels, which supports the formation of hydrophobic cavities after combination of IRG with nb. These nanopores could be of benefit in water treatment or energy applications, where nanoporous materials such as zeolites, protein crystals or metal-organic are frequently used due to their superior surface area.[42]

This nanoporous internal structure was further studied by SANS **(**Figure 3**C**). The scattering intensity of both covalent and non-covalent hydrogels increased in the low q region confirming the formation of large structures. However, while the increase follows a power-law for chemically crosslinked CS-nb hydrogels, CS-nb-*endo* and -*exo* hydrogels present a small shoulder, characteristic of a second length scale in the material. The scattering of a hydrogel is typically described by the combination of a liquid-like ($I_L(q)$) and a solid-like ($I_S(q)$) scattering terms, modelling the polymer chain in solution and the crosslinking points respectively:

$$I_{gel}(q) = I_L(q) + I_S(q) \tag{4}$$

The polymer contribution $I_L(q)$ is usually given by a Lorentzian function:

$$I_L(q) = \frac{I_L(0)}{1+\xi^2 q^2} \tag{5}$$

where ξ is the correlation length, which represents the mesh size of the gel network. It has been shown that in hydrogen-bond rich networks, such as polysaccharides, the Lorentzian exponent can be corrected with the mass fractal of the system D.[43]

For an ideal homogeneous crosslink hydrogel, the mesh size is the only characteristic length of the network internal structure, representing the distance between crosslinking points; tetra-arm PEGs[44] or click hydrogels[45] for instance are generally considered as ideal networks. In practice, inhomogeneities arise from incomplete crosslinking or the formation of highly reticulated regions of high scattering.[46] These inhomogeneities are traditionally described by an additional Gaussian term,[46, 47] an exponential function,[48] or by the Debye-Buesche-Anderson equation.[49]

The scattering intensity of both non-covalent hydrogels was best modelled by the incorporation of a Guinier-like term as first reported by Shibayama *et al*.[50] for the solid-like behaviour and with a corrected liquid-like description accounting for the hydrogen bonding, as proposed in the mechanism above:[43]

$$I(q) = \frac{I_L(0)}{\left(1 + \frac{D+1}{3}\xi^2 q^2\right)^{D/2}} + I_s(0)e^{-\frac{R_g^2 q^2}{3}} + background \quad (6)$$

where R_g is related to the aggregate dimension. Fitting the scattering data to Equation 6 suggested that both hydrogels had comparable mesh sizes of ~ 26 nm, whilst with aggregate dimensions ~ 55 nm for CS-nb-*exo* and ~ 100 nm for CS-nb-*endo* which could correspond to the nanopore dimensions in their swollen state. The mass fractal D was ~ 2.6 at the origin but quickly increased to ~ 3 over a larger q range, consistent with the presence of small, swollen objects. These observations are consistent with mesh size values obtained by rheology (ξ ~ 50 nm) and the pore size values measured by SEM (d_p ~ 60 nm in the dry state), where the heterogeneity of the gels resulting from the polydispersity of CS and its random functionalisation must be kept in mind (**Table 1**).

The scattering of the covalent hydrogel on the other hand was best fitted by including a Porod scattering term to describe the clusters:

$$I(q) = \frac{A}{q^D} + \frac{C}{1+(q\xi)^m} + background \quad (7)$$

where D is the Porod exponent of the system, m is the Lorentzian exponent, ξ is the correlation length, and A, C and the background are constants.[45, 51] Fitting data to Equation 7 yielded a mesh size of 19 nm, much smaller than for the non-covalent networks, consistent with its much higher G' (**Figure 3B**) and smaller swelling ratio (**Figure 3C**) as compared to the non-covalent gels, and

Table 1. Comparative dimensional characteristics of the hydrogel networks obtained from rheology, SEM and SANS

	Rheology	**SEM**	**SANS**			
	ξ_a (nm)	d_p (nm)	R_g (nm)	D	ξ (nm)	$/\chi^2$
Covalent	18.4	-	-	2.43	18.4 ± 3.2	12.5
-endo	53.5	66 ± 10	120 ± 22	3.18	26.2 ± 2.3	1.95
-exo	46.2	53 ± 17	52 ± 1.4	3.05	27.1 ± 0.8	6.10

a fractal dimension comprised between 2 and 3, characteristic of hydrogels. Finally, the Lorentzian exponent of 1.4 is typical of polymer chains in a good solvent, as anticipated for a hydrogel. [14] This difference in the modelling of the scattering intensity supports the structural diversity of both covalent and non-covalent networks.

Self-assembled *microgels* were also successfully synthesised from both CS-nb-*endo* and -*exo* using a nano-emulsion template.[32] The new CS-nb-*endo* and -*exo* microgels presented a hydrodynamic diameter of ~ 100 nm and ~ 150 nm, respectively, as measured by SEM and DLS (**Figure 5A-B**). They exhibited a ζ potential of + 30 mV in water, consistent with a weak polybase behaviour. In addition, CS microgels could be post-functionalised through unreacted nb moieties by tetrazine ligation, as demonstrated through a model reaction involving a self-quenching fluorescent tetrazine, Tet-Coum, which increases fluorescence upon reaction with alkenes (**Figure S12**).[52] After as little as 1 min, the fluorescence of Tet-Coum doubled, confirming the reactivity of nb moieties and demonstrated the late-stage functionalisation potential of the microgels. Interestingly, the fluorescence increase was faster and greater for CS-nb-*endo* microgels,

consistent with the lower reactivity of this diastereoisomer towards IRG radicals which leads to more unreacted nb groups that can be functionalized at the later stage.

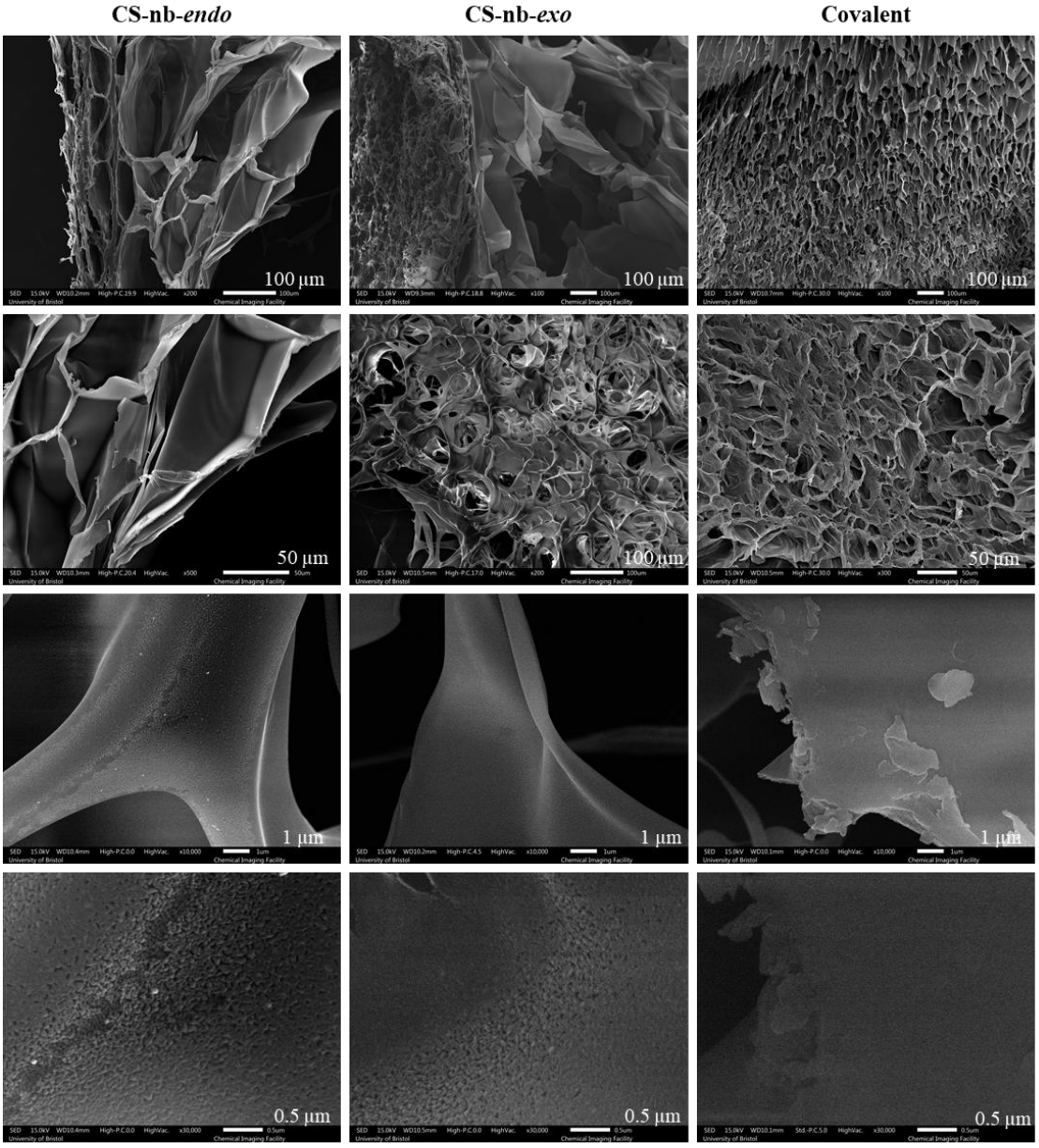

Figure 4. SEM images of CS-nb-*endo*, -*exo*, and covalent hydrogels.

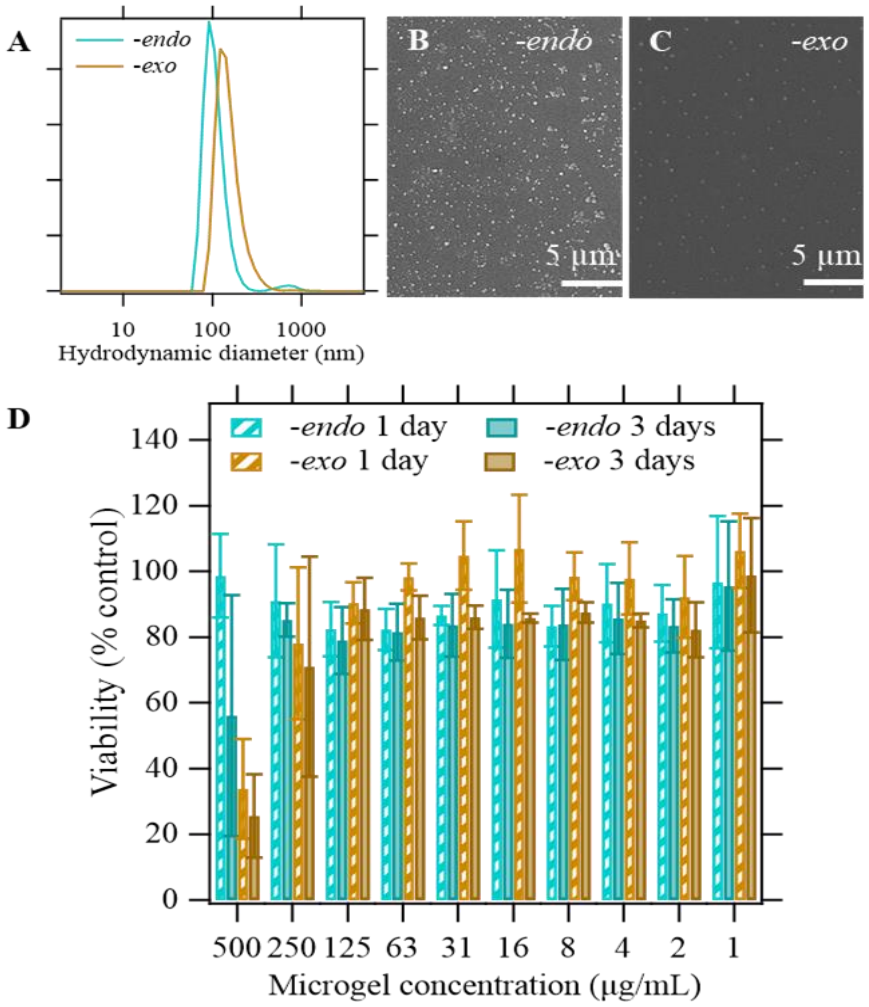

Figure 5. Characterisation of CS-nb-*endo* and -*exo* microgels: DLS (**A**), SEM (**B**, **C**) and cell viability after 1and 3 days (**D**).

The cytotoxicity of both microgels was then assessed against human dermofibroblast (HDF) cell lines exposed to microgel concentrations varied between 1 to 500 µg/mL for 1 to 3 days. Both the cell viability, assessed with Calcein AM (**Figure 5D**), and the metabolic activity, measured with Alamar Blue (AB) (**Figure S13**), were non-significantly different from the controls, especially for the -*endo* microgels, where viabilities were greater than 90 % even after 3 day exposures and for concentrations up to 250 µg/mL. CS-nb-*exo* microgels presented a higher toxicity profile at high concentrations, but viabilities of ~ 90 % were obtained after 3 days for microgel concentrations of up to 125 µg/mL. These microgels were not internalised inside cells, as evidenced by widefield microscopy tracking of the fluorescent Eosin-labelled microgels by (see ESI for synthesis details and **Figure S14**).

CONCLUSIONS

In conclusion, a new series of photo-initiated, non-covalently self-assembled hydrogels and microgels were obtained from norbonene-derived chitosan polysaccharides by recombination of IRG radicals with the norbornene alkene group, followed by hydrophobicity-driven supramolecular assembly. The resulting hydrogels were injectable and presented a nanoporous structure with internal pore diameters of ~ 50 – 100 nm. The rheological properties of the hydrogels could be tuned between ~ 20 and ~ 800 Pa depending on the polymer concentration and on the stereochemistry of carbic anhydride used to endow CS with the nb functionality. An increase in the *endo* composition of CS-nb led to weaker hydrogels of bigger nanopore diameters compared to their *exo*- counterpart. This novel photo-initiated self-assembly mechanism was also successfully applied to the synthesis of microgels. We demonstrated that the microgels could be further functionalised through their unreacted nb moieties and did not exhibit any toxicity to HDF

cells after 3-day exposures. To the best of our knowledge, this is the first report of non-covalent hydrogels and microgels via photo-initiated self-assembly based on a non-photoswitchable moiety. Compared to azobenzene switches, the synthesis is facile and the gels are stable *in vitro* as no retro-isomerisation is possible. Although only demonstrated with CS here, this strategy should be broadly applicable to other nb-functionalised polymers. In addition, the nanopores present in these hydrogels should provide the materials with improved loading properties, with possible applications in the field of drug delivery or depollution.

AUTHOR INFORMATION

Corresponding Author

*M. Carmen Galan m.c.galan@bristol.ac.uk and Wuge Briscoe Wuge.Briscoe@bristol.ac.uk

Author Contributions

S.M. performed all of the experiments and data analysis. The manuscript was written through contributions of all authors. All authors have given approval to the final version of the manuscript.

Funding Sources

We acknowledge the ISIS Muon and Neutron Source for the awarded beamtime under experiment numbers: RB 1820037; data available under 10.5286/ISIS.E.100170413. S.M. is supported by the European Research Council (ERC−COG: 648239) and the Bristol Chemical Synthesis Centre for Doctoral Training (Engineering and Physical Science Research Council (EPSRC) EP/L015366/1). SEM studies were carried out in the Chemical Imaging Facility, University of Bristol with equipment funded by EPSRC under Grant "Atoms to Applications" (EP/K035746/1).

ACKNOWLEDGMENT

We thank Professor Craig Butts for helpful discussions on the NMRs, Paul Lehman for help with the NMR. We are indebted to the members of the Galan and Briscoe groups for helpful discussions on various aspects of synthesis and characterization, in particular to Lauren Matthews for assistance on the SANS beamline.

REFERENCES

1. Strandman, S.; Zhu, X. X., Self-Healing Supramolecular Hydrogels Based on Reversible Physical Interactions. *Gels* **2016,** *2* (2), 16.
2. Ferreira, N. N.; Ferreira, L. M. B.; Cardoso, V. M. O.; Boni, F. I.; Souza, A. L. R.; Gremião, M. P. D., Recent advances in smart hydrogels for biomedical applications: From self-assembly to functional approaches. *European Polymer Journal* **2018,** *99*, 117-133.
3. Chu, C.-W.; Ravoo, B. J., Hierarchical supramolecular hydrogels: self-assembly by peptides and photo-controlled release via host–guest interaction. *Chemical Communications* **2017,** *53* (92), 12450-12453.
4. Ryan, D. M.; Nilsson, B. L., Self-assembled amino acids and dipeptides as noncovalent hydrogels for tissue engineering. *Polymer Chemistry* **2012,** *3* (1), 18-33.
5. Hsieh, F.-Y.; Tseng, T.-C.; Hsu, S.-h., Self-healing hydrogel for tissue repair in the central nervous system. *Neural Regeneration Research* **2015,** *10* (12), 1922-1923.
6. Yang, L.; Li, Y.; Gou, Y.; Wang, X.; Zhao, X.; Tao, L., Improving tumor chemotherapy effect using an injectable self-healing hydrogel as drug carrier. *Polym. Chem.* **2017**.
7. Arakawa, H.; Takeda, K.; Higashi, S. L.; Shibata, A.; Kitamura, Y.; Ikeda, M., Self-assembly and hydrogel formation ability of Fmoc-dipeptides comprising α-methyl-L-phenylalanine. *Polymer Journal* **2020**.
8. Chang, H.; Li, C.; Huang, R.; Su, R.; Qi, W.; He, Z., Amphiphilic hydrogels for biomedical applications. *Journal of Materials Chemistry B* **2019,** *7* (18), 2899-2910.
9. Tan, S.; Ladewig, K.; Fu, Q.; Blencowe, A.; Qiao, G. G., Cyclodextrin-Based Supramolecular Assemblies and Hydrogels: Recent Advances and Future Perspectives. *Macromolecular Rapid Communications* **2014,** *35* (13), 1166-1184.
10. Yang, Q.; Wang, P.; Zhao, C.; Wang, W.; Yang, J.; Liu, Q., Light-Switchable Self-Healing Hydrogel Based on Host–Guest Macro-Crosslinking. *Macromolecular Rapid Communications* **2017,** *38* (6), 1600741-n/a.
11. Qin, C.-G.; Lu, C.-X.; Ouyang, G.-W.; Qin, K.; Zhang, F.; Shi, H.-T.; Wang, X.-H., Progress of Azobenzene-based Photoswitchable Molecular Probes and Sensory Chips for Chemical and Biological Analysis. *Chinese Journal of Analytical Chemistry* **2015,** *43* (3), 433-443.
12. Pang, J.; Gao, Z.; Zhang, L.; Wang, H.; Hu, X., Synthesis and Characterization of Photoresponsive Macromolecule for Biomedical Application. *Front Chem* **2018,** *6*, 217-217.
13. Sun, N.; Wang, T.; Yan, X., Synthesis and investigation of a self-assembled hydrogel based on hydroxyethyl cellulose and its in vitro ibuprofen drug release characteristics. *RSC Advances* **2017,** *7* (16), 9500-9511.

14. Cao, X.; Peng, X.; Zhong, L.; Sun, R., Multiresponsive Hydrogels Based on Xylan-Type Hemicelluloses and Photoisomerized Azobenzene Copolymer as Drug Delivery Carrier. *Journal of Agricultural and Food Chemistry* **2014,** *62* (41), 10000-10007.
15. Patnaik, S.; Sharma, A. K.; Garg, B. S.; Gandhi, R. P.; Gupta, K. C., Photoregulation of drug release in azo-dextran nanogels. *International Journal of Pharmaceutics* **2007,** *342* (1), 184-193.
16. Wen, Y.; Oh, J. K., Recent Strategies to Develop Polysaccharide-Based Nanomaterials for Biomedical Applications. *Macromolecular Rapid Communications* **2014,** *35* (21), 1819-1832.
17. Khan, F.; Ahmad, S. R., Polysaccharides and Their Derivatives for Versatile Tissue Engineering Application. *Macromolecular Bioscience* **2013,** *13* (4), 395-421.
18. Zhu, T.; Mao, J.; Cheng, Y.; Liu, H.; Lv, L.; Ge, M.; Li, S.; Huang, J.; Chen, Z.; Li, H.; Yang, L.; Lai, Y., Recent Progress of Polysaccharide-Based Hydrogel Interfaces for Wound Healing and Tissue Engineering. *Advanced Materials Interfaces* **2019,** *6* (17), 1900761.
19. Basu, A.; Kunduru, K. R.; Abtew, E.; Domb, A. J., Polysaccharide-Based Conjugates for Biomedical Applications. *Bioconjugate Chemistry* **2015,** *26* (8), 1396-1412.
20. Radhakrishnan, J.; Subramanian, A.; Krishnan, U. M.; Sethuraman, S., Injectable and 3D Bioprinted Polysaccharide Hydrogels: From Cartilage to Osteochondral Tissue Engineering. *Biomacromolecules* **2017,** *18* (1), 1-26.
21. Dragan, E. S.; Dinu, M. V., Polysaccharides constructed hydrogels as vehicles for proteins and peptides. A review. *Carbohydrate Polymers* **2019,** *225*, 115210.
22. Plamper, F. A.; Richtering, W., Functional Microgels and Microgel Systems. *Accounts of Chemical Research* **2017,** *50* (2), 131-140.
23. McClements, D. J., Designing biopolymer microgels to encapsulate, protect and deliver bioactive components: Physicochemical aspects. *Advances in Colloid and Interface Science* **2017,** *240*, 31-59.
24. Richtering, W.; Saunders, B. R., Gel architectures and their complexity. *Soft Matter* **2014,** *10* (21), 3695-3702.
25. Kasaai, M. R., Determination of the degree of N-acetylation for chitin and chitosan by various NMR spectroscopy techniques: A review. *Carbohydrate Polymers* **2010,** *79* (4), 801-810.
26. Hao, C.; Wang, W.; Wang, S.; Zhang, L.; Guo, Y., An Overview of the Protective Effects of Chitosan and Acetylated Chitosan Oligosaccharides against Neuronal Disorders. *Marine Drugs* **2017,** *15* (4), 89.
27. Croisier, F.; Jérôme, C., Chitosan-based biomaterials for tissue engineering. *European Polymer Journal* **2013,** *49* (4), 780-792.
28. Bernkop-Schnürch, A.; Dünnhaupt, S., Chitosan-based drug delivery systems. *European Journal of Pharmaceutics and Biopharmaceutics* **2012,** *81* (3), 463-469.
29. Bhattarai, N.; Gunn, J.; Zhang, M., Chitosan-based hydrogels for controlled, localized drug delivery. *Adv Drug Deliv Rev* **2010,** *62* (1), 83-99.
30. Sahariah, P.; Másson, M., Antimicrobial Chitosan and Chitosan Derivatives: A Review of the Structure–Activity Relationship. *Biomacromolecules* **2017,** *18* (11), 3846-3868.
31. Liu, H.; Wang, C.; Li, C.; Qin, Y.; Wang, Z.; Yang, F.; Li, Z.; Wang, J., A functional chitosan-based hydrogel as a wound dressing and drug delivery system in the treatment of wound healing. *RSC Advances* **2018,** *8* (14), 7533-7549.
32. Michel, S. E. S.; Dutertre, F.; Denbow, M. L.; Galan, M. C.; Briscoe, W. H., Facile Synthesis of Chitosan-Based Hydrogels and Microgels through Thiol–Ene Photoclick Cross-Linking. *ACS Applied Bio Materials* **2019,** *2* (8), 3257-3268.

33. Ooi, H. W.; Mota, C.; ten Cate, A. T.; Calore, A.; Moroni, L.; Baker, M. B., Thiol–Ene Alginate Hydrogels as Versatile Bioinks for Bioprinting. *Biomacromolecules* **2018,** *19* (8), 3390-3400.
34. Sornkamnerd, S.; Okajima, M. K.; Kaneko, T., Tough and Porous Hydrogels Prepared by Simple Lyophilization of LC Gels. *ACS Omega* **2017,** *2* (8), 5304-5314.
35. Wisniewska, M. A.; Seland, J. G.; Wang, W., Determining the scaling of gel mesh size with changing crosslinker concentration using dynamic swelling, rheometry, and PGSE NMR spectroscopy. **2018,** *135* (45), 46695.
36. Guaresti, O.; García–Astrain, C.; Aguirresarobe, R. H.; Eceiza, A.; Gabilondo, N., Synthesis of stimuli–responsive chitosan–based hydrogels by Diels–Alder cross–linking `click´ reaction as potential carriers for drug administration. *Carbohydrate Polymers* **2018,** *183*, 278-286.
37. Heenan, R. K.; Rogers, S. E.; Turner, D.; Terry, A. E.; Treadgold, J.; King, S. M., Small Angle Neutron Scattering Using Sans2d. *Neutron News* **2011,** *22* (2), 19-21.
38. Li, S.; Wang, L.; Yu, X.; Wang, C.; Wang, Z., Synthesis and characterization of a novel double cross-linked hydrogel based on Diels-Alder click reaction and coordination bonding. *Materials Science and Engineering: C* **2018,** *82*, 299-309.
39. Wignall, G. D.; Bates, F. S., Absolute calibration of small-angle neutron scattering data. **1987,** *20* (1), 28-40.
40. Xu, Y.-M.; Li, K.; Wang, Y.; Deng, W.; Yao, Z.-J., *Mononuclear Nickel(II) Complexes with Schiff Base Ligands: Synthesis, Characterization, and Catalytic Activity in Norbornene Polymerization*. 2017; Vol. 9, p 105.
41. Chang, C.; He, M.; Zhou, J.; Zhang, L., Swelling Behaviors of pH- and Salt-Responsive Cellulose-Based Hydrogels. *Macromolecules* **2011,** *44* (6), 1642-1648.
42. Ng, E.-P.; Mintova, S., Nanoporous materials with enhanced hydrophilicity and high water sorption capacity. *Microporous and Mesoporous Materials* **2008,** *114* (1), 1-26.
43. Horkay, F.; Hecht, A. M.; Mallam, S.; Geissler, E.; Rennie, A. R., Macroscopic and microscopic thermodynamic observations in swollen poly(vinyl acetate) networks. *Macromolecules* **1991,** *24* (10), 2896-2902.
44. Shibayama, M., Exploration of Ideal Polymer Networks. **2017,** *372* (1), 7-13.
45. Saffer, E. M.; Lackey, M. A.; Griffin, D. M.; Kishore, S.; Tew, G. N.; Bhatia, S. R., SANS study of highly resilient poly(ethylene glycol) hydrogels. *Soft Matter* **2014,** *10* (12), 1905-1916.
46. Gomes, C.; Dias, R. C. S.; Costa, M. R. P. F. N., Static Light Scattering Monitoring and Kinetic Modeling of Polyacrylamide Hydrogel Synthesis. **2019,** *7* (4), 237.
47. Chalal, M.; Ehrburger-Dolle, F.; Morfin, I.; Bley, F.; Aguilar de Armas, M.-R.; López Donaire, M.-L.; San Roman, J.; Bölgen, N.; Pişkin, E.; Ziane, O.; Casalegno, R., SAXS Investigation of the Effect of Temperature on the Multiscale Structure of a Macroporous Poly(N-isopropylacrylamide) Gel. *Macromolecules* **2010,** *43* (4), 2009-2017.
48. Mallam, S.; Horkay, F.; Hecht, A. M.; Rennie, A. R.; Geissler, E., Microscopic and macroscopic thermodynamic observations in swollen poly(dimethylsiloxane) networks. *Macromolecules* **1991,** *24* (2), 543-548.
49. Hyland, L. L.; Taraban, M. B.; Feng, Y.; Hammouda, B.; Yu, Y. B., Viscoelastic properties and nanoscale structures of composite oligopeptide-polysaccharide hydrogels. *Biopolymers* **2012,** *97* (3), 177-88.

50. Shibayama, M.; Tanaka, T.; Han, C. C., Small angle neutron scattering study on poly(N-isopropyl acrylamide) gels near their volume-phase transition temperature. **1992,** *97* (9), 6829-6841.
51. Hammouda, B.; Ho, D. L.; Kline, S., Insight into Clustering in Poly(ethylene oxide) Solutions. *Macromolecules* **2004,** *37* (18), 6932-6937.
52. Devaraj, N. K.; Hilderbrand, S.; Upadhyay, R.; Mazitschek, R.; Weissleder, R., Bioorthogonal Turn-On Probes for Imaging Small Molecules inside Living Cells. **2010,** *49* (16), 2869-2872.